Supercritical Antisolvent Precipitation of TiO_2 with Tailored Anatase/Rutile Composition for Applications in Redox Catalysis and Photocatalysis

Raimon P. Marin[a], Satoshi Ishikawa[b], Hasliza Bahruji[a], Greg Shaw[a], Simon A. Kondrat[a], Peter J. Miedziak[a], Davied J. Morgan[a], Stuart H. Taylor[a], Jonathan K. Bartley[a], Jennifer K. Edwards[a], Michael Bowker[a,c], Wataru Ueda[b] and Graham J. Hutchings*[a]

[a] Cardiff Catalysis Institute, School of Chemistry, Cardiff University, Main Building, Park Place, Cardiff, CF10 3AT, UK

[b] Catalysis Research Centre, Hokkaido University, Kita 21 Nishi 10, Sapporo, Japan

[c] Rutherford Appleton Laboratory, UK Catalysis Hub, Research Complex at Harwell (RCaH), Harwell, Oxon, OX11 0FA, UK

* Corresponding author: email hutch@cf.ac.uk, phone 029 2087 4059

Abstract

TiO_2 with tailored anatase/rutile composition has been prepared from the supercritical antisolvent (SAS) precipitation of a range of titanium alkoxides. The calcination of the SAS TiO_2 was monitored by *in situ* powder X-ray diffraction to determine the optimal calcination conditions for the formation of a mixed anatse/rutile phase TiO_2. The SAS precipitated material calcined at 450 °C produced a predominantly anatase support while calcination at 750 °C resulted in a 90 wt% anatase and 10 wt% rutile TiO_2. 5 wt% AuPd was added to the SAS TiO_2 using an impregnation technique, with exceptional dispersion of the metals being observed by transmission electron microscopy. Mean metal particle sizes were determined to be below 1 nm for both anatase and anatase/rutile SAS TiO_2 materials. These catalysts were found to be highly active for the selective oxidation of benzyl alcohol and the direct synthesis of hydrogen peroxide. In addition the anatase/rutile SAS TiO_2 was found to have comparable activity to commercial anatase/rutile mixed phase TiO_2 for the photocatalytic splitting of water for hydrogen production.

Keywords

TiO_2, supercritical CO_2, photocatalysis, direct synthesis of hydrogen peroxide, alcohol oxidation

Introduction

Heterogeneous catalysis is a key tenant of green chemistry and modern life, with direct involvement in the remediation of hazardous compounds, in addition to the manufacture of many bulk and fine chemicals. The use of catalysts in processes is fundamentally green, facilitating the replacement of stoichiometric reagents, enhanced reaction rates and improved atom efficiency.

Heterogeneous photocatalysis has become a promising green technology for contributing to global energy demand and for environmental remediation. Photocatalysis offers a sustainable source of energy by taking full advantage of sunlight to drive chemical reactions using semiconductors to harvest the photon flux from solar energy to generate an electron-hole pair. During light excitation, an electron is promoted into the conduction band of a semiconductor leaving a hole in the valence band. The photogenerated electron migrates to the surface and is trapped by water or organic substrates. The most promising semiconductor that offers stability, high activity and low toxicity is TiO_2, with a 3.2 eV band gap energy that is able to adsorb photons with the wavelength less than ~380 nm. Fujishima and Honda initiated the interest in photocatalytic water splitting as a sustainable route to produce H_2 [1] with promising activity demonstrated for TiO_2 impregnated with noble metal co-catalysts such as Pd and Pt [2].

Gold dispersed on metal oxide supports has been shown to be effective for the selective oxidation of carbon monoxide [3,4], alcohols[5], alkenes[6,7] and the direct synthesis of hydrogen peroxide[8]. Alloying of gold with palladium and platinum has been shown in multiple studies to enhance activities and selectivities for alcohol oxidations [9-11] and increase hydrogen peroxide yields in the direct synthesis reaction [12-14].

The catalytic properties of these gold and gold alloy supported catalysts have been shown to be highly dependent on the support material and the procedure used to deposit the metal. A multitude of methods, including various wet impregnation [15-17], deposition precipitation [9,18], sol-immobilisation[19], vapour deposition [20] and mechanochemical [21] methods have been shown to give different metal particle sizes, alloy compositions and metal-support interactions. Analogous changes in particle composition and morphology can be achieved with different metal oxide and carbon supports [22]. In addition, metal oxide supports themselves can dramatically change activity [23] and reaction selectivity profiles, with the latter shown in a study by Sankar *et.al.* where the undesired production of toluene in the oxidation of benzyl alcohol could be eliminated by using supports with basic sites, such as MgO and ZnO [24].

A multitude of procedures for making metal oxide supports have also been reported [25]. The effect of the different support synthesis methods are often observed as differences in the crystalline phases, morphology, surface area, porosity, crystallite size and the number of defect sites. These support properties can have a dramatic influence on the catalytic properties of noble metal supported catalysts, as observed by Corma *et. al.* for Au/CeO_2 catalysed CO oxidation [26, 27]. It was found that nanocrystalline CeO_2 greatly enhanced the activity of the catalysts for CO oxidation when compared to CeO_2 comprised of larger crystallites. More recently we have demonstrated that Au and AuPd supported on CeO_2 catalysts prepared by supercritical anti-solvent (SAS) precipitation had exceptional activity for both CO oxidation [28] and the solvent free oxidation of benzyl alcohol [29].

The high activity of these SAS catalysts was attributed to the exceptional dispersion of Au and Pd facilitated by the highly defective CeO_2 produced by the SAS technique.

Further studies into oxidation catalysts synthesised using SAS precipitation, such as vanadium posphates, Co_3O_4 and $CuMnO_4$, have shown that poorly crystalline nanocrystalline materials with good redox properties and high activity for a range of reactions [30-32]. Studies have also been performed on the SAS preparation of TiO_2 in both batch and semi-continuous modes using acetylacetonate and alkoxide precursors [33-36]. These studies include the use of supercritical CO_2 to induce hydrolysis of alkoxides [33] and also to facilitate the polymerisation of alkoxides with acetic acid, akin to a sol-gel process [36]. Calcination of these precursors has resulted in various TiO_2 morphologies and significantly different anatase/rutile compositions. However, with the exception of one investigation into CO oxidation using Au/TiO_2 catalysts prepared by SAS precipitation of titanium acetylacetonate [37], these studies have not explored the potential of the prepared TiO_2 for catalytic applications.

Here we show the SAS preparation of TiO_2 from titanium alkoxides and titanium acetylacetonate, the optimisation of the calcination conditions and a comparison of the resulting materials performance as a catalyst support for the photocatalytic splitting of water, the selective oxidation of benzyl alcohol and the direct synthesis of hydrogen peroxide. We report for the first time the polymerisation of titanium alkoxides with acetic acid in a SAS continuous set up and their use as catalyst support precursors.

Experimental

Preparation of TiO_2 support

Initial studies into the effect of using different titanium alkoxides and titanium acetylacetonate precursors (listed in Table 1) was performed using a small scale SAS reactor, described in detail previously [38]. The following provides a summary of the SAS procedure: A precursor solution was prepared containing 30 mg ml^{-1} of titanium salt dissolved in 2 vol% H_2O/MeOH and 0.01 g ml^{-1} acetic acid to prevent alkoxide hydrolysis in solution. This solution was then pumped at 0.5 ml min^{-1} into a precipitation vessel held at 40 °C, 120 bar. CO_2 (BOC), was pumped concurrently at 12 l min^{-1}. Contact between the precursor solution and the supercritical CO_2 results in rapid extraction of the solvent and precipitation of the precursor. The precipitation was carried out for an hour, before the system was flushed with CO_2 to remove residual solvent on the precipitate. The apparatus was depressurised and the precipitate recovered, characterised and then calcined to form the TiO_2. The most promising materials were then prepared on a larger scale using apparatus manufactured by Separex using the same temperature and pressure but with higher solvent and CO_2 flow rates to produce a greater quantity of product [31].

Preparation of catalysts

Supported metal catalysts were then prepared using the SAS precipitated TiO_2 materials as the support. Catalysts were also prepared on P-25 (Degussa) and anatase (Sigma Aldrich 99.8%) standards. 0.5 wt% Pt/TiO_2 photocatalysts were prepared by impregnation with an aqueous solution of 10 mg ml^{-1} H_2PtCl_6 (Alfa Aesar 99.9%). The resultant slurry was then dried in an oven at 120 °C for 2 h before being calcined at 300 °C for 3 h. 2.5 wt% Au-2.5 wt% Pd/TiO_2 catalysts were used for

alcohol oxidation and the direct synthesis of hydrogen peroxide and these were prepared by wet impregnation using $HAuCl_4$ and $PdCl_2$ (Alfa Aesar). The resultant slurry was dried at 110°C for 16 h before being calcined at 400 °C for 2h.

Characterisation

The SAS precipitated materials, supports following calcination and final catalysts were characterised using a combination of infrared spectroscopy, X-ray diffraction, thermogravimetric analysis,

Diffuse reflectance infrared Fourier transform spectroscopy (DRIFTS) was carried out using a Bruker Tensor 27 spectrometer equipped with a Harrick praying mantis cell and MCT detector. Surface areas were determined by multi-point N_2 adsorption at 77 K using a Micromeretics Gemini 2360 instrument according to the Brauner Emmet Teller method. Transmission electron microscopy (TEM) was performed using a Jeol 2100 microscope fitted with a LaB_6 filament operating at 200 kV. Samples were prepared by dispersing the powder catalyst in ethanol and dropping the suspension onto a lacey carbon film over a 300 mesh copper grid. Thermal gravimetric analysis (TGA) was performed using a SETARAM Labsys thermogravimetric analyser using 100 µl alumina crucibles.

Powder X-ray diffraction (XRD) was performed using a PANalytical X'Pert Pro diffractometer fitted with a monochromatic Cu Kα source (λ = 0.154 nm) operated at 40 kV and 40 mA. The scans were recorded in the 2θ range 10-80° using a step size of 0.016° and scan step time of 55 seconds. Anatase (ICDD 03-065-5714) (X_A) and rutile (ICDD 03-065-1118) (X_R) phase composition was determined using the relative intensity ratio method with the following equation. $X_A = 1 / (1+1.26 (I_R / I_A))$, where I_R is the intensity of the rutile (110) reflection and I_A is the intensity of the anatase (101) reflection.

To study the calcination temperature dependence on rutile formation, SAS prepared TiO_2 precursors, which had been pre-calcined at 400 °C for 2h, were heated to 750 °C and monitored using an X'pert Pro XRD with an Anton-Parr XRK900 *in situ* cell. Experiments were performed under a flow of 1 ml min^{-1} air to replicate the conditions in the tube furnace used for the *ex situ* calcination. Two sets of in situ XRD experiments were performed. Initial experiments under conditions that replicated the TGA (heating to 750 °C) with diffraction patterns collected every 25°C from 23-30°, and a heating rate of 10 °C min^{-1}. The second set of isothermal experiments, with 10-80 °2θ scans, were then performed at the various temperatures of 450, 650, 700 and 750 °C. Scans were continuously taken in the isothermal experiments, with each scan taking 30 min (i.e each data point is at 30 increments). Flow and ramp rates were the same for all experiments.

Catalyst testing

Photocatalytic water splitting

Liquid phase photocatalytic water splitting experiments were carried out using methanol as sacrificial agent to enhance hydrogen production. The catalyst (0.2 g), methanol (100 µl, Aldrich 99.9%) and water (deionised, 100 ml) were added directly to the stirred reaction vessel. The methanol/water mixture was purged with Ar for 30 minutes to remove air and the flask illuminated by a 400 W Xe arc lamp (Oriel model 66921). Gas samples were taken every 30 min and analysed

using a Varian 3900 GC fitted with a 2 m MS 13X column. Control experiments were carried out under identical conditions, but in the absence of the catalyst no significant hydrogen evolution was observed.

Benzyl alcohol oxidation

Catalyst testing was performed using a stainless steel autoclave (Autoclave Engineers In-line MagneDrive III) with a nominal volume of 100 ml and a maximum working pressure of 140 bar . The vessel was charged with benzyl alcohol (40 ml) and catalyst (25 mg). The autoclave was then purged three times with oxygen leaving the vessel at 10 bar. The pressure was maintained at a constant level throughout the experiment; as the oxygen was consumed in the reaction, it was replenished. The stirrer speed was set at 1500 r.p.m. and the reaction mixture was raised to the required temperature of 140 °C. Samples from the reactor were taken periodically *via* a sampling pipe, ensuring that the volume purged before sampling was higher than the tube volume, and analysed by GC (Varian 3800) using a CP-wax column.

Direct H_2O_2 synthesis

Synthesis of H_2O_2 from H_2 and O_2 was performed using a Parr Instruments stainless steel autoclave with a nominal volume of 100 mL and a maximum working pressure of 140 bar. The reactor was charged with CH_3OH (5.6 g), H_2O (2.9 g) and catalyst (0.01 g). The charged autoclave was then purged three times with 5% H_2/CO_2 (7 bar) before filling with 5% H_2/CO_2 to a pressure of 29 bar at 20 °C. This was followed by the addition of 11 bar of 25% O_2/CO_2. The reactor was then cooled to 2 °C and the reaction started with stirring at 1200 rpm. The reaction was then carried out for 30 min. The amount of hydrogenated H_2O_2 was determined by titrating aliquots with acidified $Ce(SO_4)_2$ (0.0288 M) in the presence of a ferroin indicator.

H_2O_2 hydrogenation

Hydrogen peroxide hydrogenation was evaluated using the same Parr Instruments stainless steel autoclave. To test each catalyst for H_2O_2 hydrogenation, the autoclave was charged with catalyst (0.01 g) and a solution containing 4 wt% H_2O_2 (5.6 g CH_3OH, 2.22 H_2O and 0.68 g H_2O_2 50% wt/wt). The charged autoclave was then purged three times with 5% H_2/CO_2 (7 bar) before filling with 5% H_2/CO_2 to a pressure of 29 bar at 20 °C. The temperature was then allowed to decrease to 2 °C followed by stirring the reaction mixture (1200 rpm) for 30 min. The amount of hydrogenated H_2O_2 was determined by titrating aliquots with acidified $Ce(SO_4)_2$ (0.0288 M) in the presence of a ferroin indicator.

Results and discussion

Characterisation of SAS precipitated materials

As observed in previous studies, the SAS precipitates were all found to be amorphous, attributable to the fast nucleation rate achieved by SAS [39]. DRIFTS analysis (Figure 1) of the SAS precursors prepared from the alkoxides had clear ν_s(CCO) and ν_{as}(COO) bands at *ca.* 1540 and 1450 cm^{-1} ($\Delta\nu_{as}$-ν_s 90 cm^{-1}), along with a band at 1415 cm^{-1}, that are indicative of chelating bidentate titanium acetate

complexes [39]. The bands at *ca.* 1385 and 1050 cm^{-1} are associated with alkoxides (CH_3 deformation and *v*(Ti-O-C)), that in addition to the strong oxo bands below 800 cm^{-1}, suggest that a sol-gel condensate was produced, as seen previously [40]. Similar bands were observed in the acetylacetonate precipitate, although there were bands at 1585 cm^{-1} and 1360 cm^{-1}, that can be assigned to the original acetylacetonate ligand rather than the alkoxide [37]. In addition, there are bands associated with hydroxyl groups at *ca. 3*386 and 1630 cm^{-1} associated with water and evidence of a free carboxylic acid determined from the band at 1720 cm^{-1} in the isopropoxide sample.

Surface areas of the SAS precipitates (Table 1) were high which is typical of SAS precipitated materials, due to the high nucleation rates that leads to small (<100 nm) particles [34]. Surface areas of the poly-condensates from the alkoxides were found to be higher than the precipitate from the titanium acetylacetonate, with an observable relationship between the alkoxide chain length and the surface area of the precipitated material. This trend culminates in the highest surface area of 304 m^2g^{-1}, being observed for the ethoxide derived precursor. This surface area is comparable to that found by Sui *et. al.* in their report of the batch synthesis of TiO_2 using a CO_2 sol-gel procedure, although it is interesting to note that their operating pressure was almost 300 bar higher than in the SAS precipitation methodology [36].

Thermal gravimetric analysis (TGA) was performed on the SAS precipitates to determine an optimal calcination temperature to form TiO_2 (Figure 2). All samples showed a multiple stage decomposition, with an initial mass loss centred around 80 °C, that is attributable to the removal of residual solvent observed by DRIFTS. Two further mass losses, centred at 215 and 305 °C could be observed prior to a mass gain starting at 350 °C that must be associated with an oxidation process. The extent of this mass gain varied considerably between samples, with the ethoxide and isopropoxide samples experiencing a far less significant mass gain compared to the butoxide and acetylacetonate samples. An explanation for this could be that the mass loss events at 215 and 305 °C are associated with decomposition of acetate compounds, which are known to cause partial reduction of transition metals [21], with the subsequent mass gain due to the rapid re-oxidation of any reduced species. Finally, a high temperature mass loss was observed, with the extent and temperature depending on the precursor salt used. For the alkoxide derived samples the percentage mass loss of this final step correlated with the size of the alkyl group, the smallest mass loss being associated with the ethoxide precursor and the largest from the butoxide. The mass loss associated with the acetylacetonate precursor was the most significant of all the samples. Clearly the thermal decomposition of the SAS precipitates is highly complex, with the exact nature of many of the individual steps being difficult to assign with confidence. From the perspective of choosing an optimal calcination temperature for TiO_2 formation the onset of final mass loss, which is associated with residual organic compounds, was chosen as the calcination temperature. The highest temperature final mass loss was associated with the titanium isopropoxide derived sample starting at 450 °C, consequently all precursors were calcined at this temperature.

Characterisation of SAS TiO_2

After calcination at 450 °C the resultant TiO_2 materials were characterised by XRD to determine the phase composition and crystallite size (Figure 3 and Table 1). All the samples were found to predominately be anatase, although residual rutile (*ca.* 2 wt) was observed in the isopropoxide and

acetylacetonate derived samples, as determined by a relative intensity ratio method detailed in the experimental section. The other alkoxide derived TiO_2 materials also contain traces of rutile, but the peak area was so low that it could not be suitably fitted. The prevalence of the metastable anatase phase can be expected given the lower surface free energy and less constrained molecular construction of anatase relative to rutile, which results in this phase being frequently observed as the initial crystalline TiO_2 phase formed [41]. The observed crystallite size for the anatase phases (Table 1) showed that the smallest crystallite size was observed for the isopropoxide and acetylacetonate derived samples. It is notable that the final decomposition temperature observed by TGA (Figure 2) of these two materials was highest of those investigated. Potentially the slower evolution of the residual organics within these two samples could have slowed TiO_2 crystal growth rates and so yielded smaller crystallite sizes. Surface area of the calcined TiO_2 samples derived from the alkoxides correlate well with observed crystallite sizes from XRD, with higher surface area corresponding to lower crystallite size. The apparent exception is the acetylacetonate derived sample, which has quite a low final surface area. However, this was due to the relatively low surface area of the uncalcined SAS acetylacetonate precursor compared to the alkoxide derived samples. When looking at the percentage retention of surface area after calcination it was observed that the acetylacetonate and isopropoxide derived samples were moderately better than the other two alkoxide samples.

Photocatalytic activity

The activity of the SAS prepared TiO_2 for photocatalytic water splitting, with methanol as sacrificial agent, was performed and compared to an anatase standard. As discussed in detail in the experimental section, Pt nanoparticles were dispersed on the TiO_2 to help maintain separation of charge carriers. Figure 4 shows the volume of hydrogen produced in a 3 h reaction. TiO_2 produced from the SAS isopropoxide precursor produced the most hydrogen followed by the ethoxide derived catalyst and the anatase reference sample, which showed similar activity, whilst the catalysts derived from the butoxide and acetylacetonate salts gave very little hydrogen production (<0.1 ml of hydrogen in 3h). Degussa P-25 titania (anatase 80% rutile 20%) is a standard semiconductor commonly used in the photocatalytic water splitting reaction, and it has been proposed that its excellent activity is a result of synergistic effects occurring between the anatase and rutile phases [42, 43]. The higher activity of the TiO_2 derived from the isopropoxide precursor, relative to the anatase standard, could be associated with the relatively high surface area in conjunction with the presence of small quantities of rutile. The benefit of rutile is that it has a narrow band gap energy (3.0) eV with the conduction band being -0.2 eV below the conduction band of anatase [42]. During light excitation, rutile acts as an electron sink to accept the photogenerated electron from the anatase conduction band, thus increasing the charge carrier lifetime. The charge carrier must then travel to the surface to react, or otherwise undergo recombination. The benefit of a high surface area is that for most of the metal oxides, such as TiO_2, the surface is covered with hydroxyl groups, which are thought to play a role in enhancing surface reaction by trapping the photogenerated holes, producing OH• radicals as shown below [44].

$TiO_2 + hv \rightarrow e^- + h^+$

$h^+ + OH^- \rightarrow OH\bullet$

The number of surface hydroxyl groups is proportional to the surface area of the TiO_2, where the Ti-O dangling bond is compensated by a proton that mostly comes from water molecules during the synthesis, or when annealing at high temperature. Since the surface area of the TiO_2 produced from the SAS method vary in the range 33 – 91 $m^2 g^{-1}$, it is useful to compare the specific activity of the catalysts by normalising the volume of hydrogen produced to the surface area of the TiO_2 as shown in Figure 4b. TiO_2 produced from isopropoxide and acetylacetonate precursors have the highest surface area normalised H_2 production, consistent with the mixture of anatase and rutile crystalline phases in these catalysts. Despite the higher activity of the rutile containing catalysts it is important to note that their activity was still vastly inferior to the commonly used P-25 titania supported catalysts [42, 43].

Optimisation of SAS prepared TiO_2

Given the reasonable activity for the water splitting reaction of the TiO_2 derived from the isopropoxide precursor, we decided to optimise the calcination procedure of this precursor. The purpose of this was to increase the rutile content, as the phase composition of TiO_2 has significant consequences on the catalytic performance for photocatalysis and many other different reactions. Thermal treatment is the most common method of inducing phase change between anatase and rutile, and so the effect of calcination temperature on the phase composition of the titanium isopropoxide derived sample was investigated. Figure 5 shows the evolution of the anatase (101) and rutile (110) reflections in an *in situ* XRD study from 400 °C to 750 °C with a ramp rate of 10 °C min^{-1}, with a short 2.5 min XRD scan every 25 °C. From this initial experiment it was evident that some crystalline anatase was present at 400 °C, prior to the final mass loss observed at 450 °C by TGA. The peak area of the (101) anatase reflection then dramatically increases up to 450 °C, which correlates with the mass loss observed in the TGA, indicating increasing crystallinity of the anatase phase. The crystallinity then increases at a slower rate with a maximum (101) peak area observed at 600 °C. Above this temperature the peak area slightly decreases with increasing temperature, with an appreciable rate of change becoming apparent at temperatures above 700 °C. The loss in anatase peak area can be attributed to the growth of the rutile phase, although by 750 °C the size of the characteristic (110) rutile reflection is very small, indicating that only trace amounts of crystalline rutile were present.

As the phase transformation from anatase to rutile is reconstructive the formation is not instantaneous and will be kinetically limited. Therefore, it was not surprising that no appreciable amounts of rutile were observed during the temperature ramp experiment. However, the study does highlight potential temperatures for further investigation. Monitoring the 450 °C calcination temperature would be useful, as there is clearly an increase in the crystallinity of the sample at this temperature, but without further transformation to rutile, whilst experiments at 650, 700 and 750 °C would be expected to show the evolution of rutile at different rates. Consequently, these four temperatures were chosen for iso-thermal *in situ* XRD experiments with the resulting diffraction patterns being shown in Figure 6 and 7, with the summarised crystallite size and rutile content shown in Figure 8.

As anticipated from the initial *in situ* XRD experiment, holding the calcination temperature at 450 °C did not result in the growth of the rutile phase within the 20 h duration of the experiment, with the exception of the small amount of rutile present from the start. Peak area analysis of the anatase

(101) reflection showed an increase in crystallinity for the first 2.5 h, with crystallite size growing from an initial 12 nm to 16 nm over 5 h, after which the crystallite size stabilised. While it is generally considered that the phase transition temperature for anatase to rutile is 600-700 °C [41], there have been reports of rutile formation at temperatures as low as 465 °C in systems with very small anatase crystallite sizes (4-6 nm) [45]. The relationship between small anatase crystallites and the nucleation of rutile observed, in very pure TiO_2 systems, was attributed to small crystallites having many interfaces for rutile to nucleate on. Potentially this can explain the small amounts of rutile (*ca.* 2%) observed at the start of the reaction, as we have confirmed that there are significant amounts of poorly crystalline TiO_2 initially. However, the anatase crystallites quickly grow to larger sizes that are not conducive to rutile formation at low temperatures.

At 650 and 700 °C it was expected that there would be appreciable growth of rutile over the 20 h calcination period. However, no increase in rutile content from the initial 2 % was observed at 650 °C and a modest growth to 6% rutile was seen at 700 °C, during the 20 h experiment. In both cases the crystallite size of anatase stabilises at *ca.* 25 nm after 10 h. This can still be considered in the nanocrystalline region, so it is quite surprising that rutile growth was only observed at the upper end of the temperature range expected for macrocrystalline anatase reconstruction to rutile. Small anatase crystallites thermodynamically have a lower total free energy than rutile, due to the greater contribution of the low surface energy in nanoparticles relative to macroparticles [46]. This could potentially explain why the anatase derived from SAS precipitation has a relatively high transition temperature. However, this effect was not observed experimentally in the general literature with nanocrystallites being shown to have the opposite effect (i.e enhancing rutile formation) as discussed previously. An alternative rationale for stability of the anatase could be the effect of carbon impurities from the SAS precipitation method, although it has been predicted that carbon doping would in fact enhance phase transformation and not hinder it [41].

In contrast to the slow phase transformation observed at 700 °C, the *in situ* XRD experiment at 750 °C showed a dramatic degree of phase change within 2.5 h, with the phase composition of rutile growing to *ca.* 50 %. Most successful photo catalysts reported contain mixtures of anatase and rutile, with rutile compositions of 20 to 30%. In addition both the selective oxidation of alcohols and the direct synthesis of H_2O_2 generally use Degussa P-25 as the support (which consists of 80% anatase and 20% rutile). Therefore, the SAS prepared materials were calcined at 750 °C for 90 minutes in an attempt to produce TiO2 with a desirable rutile content. This material was then doped with 0.5 wt.% Pt and tested for the photocatalytic splitting of water and compared with the SAS Ti-isopropoxide derived material calcined at 450 °C. In addition, the 450 °C and 750 °C calcined SAS Ti-isopropoxide was tested for selective oxidation of benzyl alcohol and the direct synthesis of H_2O_2, after AuPd impregnation.

Characterisation of optimised TiO_2 catalysts

Figure 9 shows the XRD of the TiO_2 prepared from the isopropoxide precursor calcined at 450 °C and 750 °C. Interestingly, the conditions that gave *ca.* 30 wt% rutile in the *in situ* XRD cell resulted in only 10 wt% rutile when calcined in a tube furnace. This demonstrates the effect of heat treatment conditions on the phase transformation. The amount and packing of the samples were two differences that have been shown to affect the anatase to rutile phase transformation [41]. Despite

the less than expected rutile content, the 750 °C *ex situ* calcined sample still had a 5 fold increase in rutile content compared to that found from 450 °C calcination.

TEM of these TiO_2 precursors calcined at 450, 650 and 750 °C along with the uncalcined material was performed to provide information on the morphology of the materials obtained from SAS precipitation (Figure 10). As predicted from previous SAS studies, the uncalcined isopropoxide precursor comprised of ~50 nm semi-spherical particles that were bridged to form agglomerates. Interestingly this morphology mostly survives the 450 °C calcination, with no apparent growth in particle size. Another observation is the areas of light contrast observed within the particles, which can be ascribed to voids within the materials. A similar phenomenon was observed for CeO_2 prepared *via* SAS precipitation and was ascribed to densification calcination of the amorphous precursor into the crystalline phase [28]. Calcination at higher temperature (650 and 750 °C) resulted in the formation of slightly larger and more faceted particles, normally associated with TiO_2. The voids were still found to be present within these more crystalline catalysts, although their frequency decreased with increasing calcination temperature.

Figure 11 provides representative TEM images of the supports following the addition of the active metal. These catalysts can be compared with gold and palladium supported on P-25 ($AuPd/TiO_2$(P-25)), which has been reported multiple times [9, 10, 12]. $AuPd/TiO_2$(P-25) has been shown to have a bimodal metal particle size distribution, with small particles of 1-8 nm as well as large 40-70 nm particles. In contrast, no particles bigger than 2 nm were observed on the isopropoxide derived TiO_2 calcined at 450 °C ($AuPd/TiO_2$(isopropoxide-450 °C)). In fact the majority of particles observed were of a size that was on the limit of accurate quantification for the microscope used, with only a small number of definable particles. As the catalysts were prepared by an impregnation technique, the full 5 wt% metal must have been deposited, suggesting that a significant proportion of the metal is of a particle size below the detection limit of the TEM. Despite this, a sufficient number of particles could be counted to give a mean particle size of 0.8 nm, although the associated error can be expected to be quite high. Such an exceptional dispersion of metals has previously been reported for SAS prepared CeO_2 where no definable particles could be observed, but EDS analysis confirmed the presence of the metals [29]. The rational for the high dispersion on the current and previously reported SAS supports is that the process imbues the supports with a large number of surface defects that provide nucleation sites for the impregnated metals. Calcination of the SAS support at 750 °C ($AuPd/TiO_2$(isopropoxide-750 °C)) resulted in a greater number of larger discernable metal particles (up to 4nm) than observed in the 450 °C sample. However, the majority of the particles were still sub nanometer, giving a mean particle size of 1 nm. This indicates that there are still a high number of metal nucleation sites, although a smaller number than in the 450 °C calcined support.

XPS characterisation was carried out to analyse the surface composition of the different catalysts and the quantified XPS data is shown in Table 2. The Ti:O ratios for all the catalysts are lower than the expected 0.5 for stoichmetric titania, which is likely to be due to the formation of surface species such as hydroxyl groups formed in wet impregnation of metals. It was noted that the SAS prepared TiO_2 had a greater surface oxygen deficiency than P-25, which could reflect the defective nature of these materials. All Au/Pd catalysts were found to have significantly higher Pd surface concentration relative to Au, suggestive of a core shell morphology. This interpretation is not definitive, as increases in Pd/Au ratios above the nominal Pd/Au molar ratio have previously been shown not to correlate with core-shell morphologies by detailed electron microscopy [47]. Despite all catalysts

having a Pd rich surface, the Pd/Au ratio differs significantly between samples with the lowest Pd surface enrichment being observed for AuPd/TiO_2(isopropoxide-450 °C) (Pd/Au of 11.69). The Pd/Au ratio then rises dramatically for AuPd/TiO_2(isopropoxide-750 °C) to 32.27, while AuPd/TiO_2(P-25) ratio lies in-between the SAS prepared materials at 17.79.

Optimised Photocatalyst

Figure 12 shows the hydrogen production of the Pt/TiO_2 catalyst prepared using the isopropoxide derived catalyst calcined at 450 °C (Pt/TiO_2(isopropoxide-450 °C)) and 750 °C (Pt/TiO_2(isopropoxide-750 °C)), compared with a catalyst prepared using P-25 (Pt/TiO_2(P-25)). The dramatically lower activity of the predominantly anatase Pt/TiO_2(isopropoxide-450 °C) relative to Pt/TiO_2(P-25) is clear with an order of magnitude difference in the hydrogen production after 3 h. However, for the Pt/TiO_2(isopropoxide-750 °C) containing 90% anatase and 10 % rutile the photocatalyic water splitting activity increases significantly. The final volume of hydrogen produced from this catalyst was comparable to Pt/TiO_2(P-25). Interestingly the time on line data shows that the initial activity of the SAS derived material was greater than Pt/TiO_2(P-25) although there is deactivation over time. The initial high activity is interesting as the material has a lower rutile content than P-25 (10% vs 20% rutile) and also a lower surface area of 25 m^2g^{-1} compared to the 55 m^2g^{-1} for P-25. Clearly a third factor must be responsible for the high activity of the catalyst. This is most likely to be a more intimate Pt-TiO_2 interaction in the SAS prepared material, due to the high number of nucleation sites present.

AuPd/TiO_2 catalyst activity for redox reactions

Having demonstrated that the supercritical antisolvent precipitation method can be used to synthesise titania that is effective for photocatalytic water splitting, the most active materials (prepared from the isoporopoxide precursor) were also tested as conventional catalyst supports. We have previously reported gold-palladium supported on titania is an affective catalyst for both the oxidation of benzyl alcohol to benazaldyhde and the direct synthesis of hydrogen peroxide [9, 10, 12]. For comparison AuPd/TiO_2(P-25) was also tested for these reactions. The results of the oxidation of benzyl alcohol are shown in Figure 13, with AuPd/TiO_2(isopropoxide-450 °C) displaying very similar activity to catalysts supported on commercially sourced P-25, which has been reported to have particularly high turnover numbers for alcohol oxidation reactions [10]. However, isopropoxide-750 °C was, at all points of the reaction, more active than the P-25 supported catalyst. As shown in Figure 13 the selectivity towards benzaldehyde was very similar for all three catalysts tested. Whilst the activity was similar AuPd/TiO_2(isopropoxide-450 °C) and AuPd/TiO_2(P-25), the particle size distribution was quite different, suggesting that small particle size cannot be the only factor responsible for activity. In addition, it was found that AuPd/TiO_2(isopropoxide-750 °C) had a slightly larger mean particle size than AuPd/TiO_2(isopropoxide-450 °C), but it was significantly more active. Au-Pd alloy morphology could potentially have a significant effect on the activity of the

catalysts, with XPS analysis (Table 2) showing that AuPd/TiO_2(isopropoxide-750 °C)had a substantially higher Pd/Au ratio than the other catalysts.

The results of the direct synthesis of hydrogen peroxide are shown in Table 3, with a different trend to the benzyl alcohol oxidation data being observed. We have previously reported that AuPd/TiO_2(P-25) has a hydrogen peroxide product synthesis activity of 64 mol H_2O_2 mol^{-1} cat h^{-1}, while AuPd/TiO_2(isopropoxide-450 °C) had an improved activity of 135 mol H_2O_2 mol^{-1} cat h^{-1}. In contrast to the benzyl alcohol data, AuPd/TiO_2(isopropoxide-750 °C) had a lower peroxide productivity (108 mol H_2O_2 mol^{-1} cat h^{-1}), although this is still higher AuPd/TiO_2(P-25). Small particles are thought to be most active for the reaction and so the trend in productivity correlates well with the particle size distributions observed by TEM analysis. Often more active catalysts which are active for the formation of hydrogen peroxide are usually also active for the over hydrogenation to form water. To try to further understand the observed productivities, hydrogenation tests were carried out as described in the experimental section (Table 3). Under our standard hydrogenation conditions with the that AuPd/TiO_2(P-25) catalyst 12% of the starting H_2O_2 was hydrogenated, whereas only 7% of the H_2O_2 was hydrogenated over that AuPd/TiO_2(isopropoxide-450 °C), which could explain the higher productivity values. The slight reduction in observed peroxide productivity of AuPd/TiO_2(isopropoxide-750 °C) can be related to the higher H_2O_2 hydrogenation of 14%. We have previously shown that acid washing a support can lead to almost complete suppression of the hydrogenation reaction [48], and that the acid washed catalysts exhibit significantly less pure palladium sites. The XPS Pd/Au ratios of the TiO_2 catalysts (Table 2) can act as an indicator of the presence of such hydrogenating palladium species. In this case the Pd/Au ratio correlates with the hydrogenation activity of the catalysts, indicating that there are more palladium rich species on AuPd/TiO_2(P-25) and AuPd/TiO_2(isopropoxide-750 °C) than on AuPd/TiO_2(isopropoxide-450 °C). This could imply that these species are preferentially formed on the rutile phase of titania, however further studies are required to confirm this hypothesis.

Conclusion

We have prepared TiO_2 as a support for Pt and AuPd nanoparticles by precipitation with a supercritical CO_2 antisolvent. A range of titanium precursor salts were screened for their physical properties and activity for the photocatalytic splitting of water. The most successful precursor was found to be titanium isopropoxide, which gave the highest surface area and contained a mixture of anatase and rutile phases. Although this material was found to contain rutile after calcination at 450 °C, this made up only *ca.* 2 wt% of the material. Therefore, we investigated the effect of calcination temperature and duration using *in situ* XRD. It was discovered that, although a small amount of rutile could be produced at low temperature, calcination at 750 °C was required to substantially enhance rutile composition. Supported metal catalysts were prepared with the SAS precipitated titanium isopropoxide calcined at 450 °C and 750 °C, which contained 2 wt% and 10 wt% rutile respectively. Exceptional dispersion of sub nanometre AuPd was found on the SAS prepared catalyst calcined at 450 °C, and this dispersion was also present on the support calcined at 750 °C. High

activity was observed for the 10% rutile containing SAS prepared TiO_2 for the oxidation of benzyl alcohol to benzaldehyde and the photocatalytic splitting of water. While the predominantly anatase containing SAS prepared TiO_2 was found to be most active for the direct synthesis of hydrogen peroxide.

Acknowledgements

We gratefully acknowledge the UK Technology Strategy Board, the UK Catalysis Hub and the Japanese Society for the Promotion of Science.

References

[1] A. Fujishima, K. Honda, Nature 238 (1972) 37.
[2] H. Bahruji, M. Bowker, P.R. Davies, F. Pedrono, Appl. Catal. B Environ. 107 (2011) 205-209.
[3] M. Haruta, T. Kobayashi, H. Sano, N. Yamada, Chem. Lett. (1987) 405-408.
[4] P. Landon, J. Ferguson, B.E. Solsona, T. Garcia, A.F. Carley, A.A. Herzing, C.J. Kiely, S.E. Golunski, G.J. Hutchings, Chem. Commun. (2005) 3385-3387.
[5] A. Corma, M.E. Domine, Chem. Commun. (2005) 4042-4044.
[6] A.K. Sinha, S. Seelan, S. Tsubota, M. Haruta, Angew. Chem., Int. Ed. 43 (2004) 1546-1548.
[7] M.D. Hughes, Y.-J. Xu, P. Jenkins, P. McMorn, P. Landon, D.I. Enache, A.F. Carley, G.A. Attard, G.J. Hutchings, F. King, E.H. Stitt, P. Johnston, K. Griffin, C.J. Kiely, Nature 437 (2005) 1132-1135.
[8] P. Landon, P.J. Collier, A.J. Papworth, C.J. Kiely, G.J. Hutchings, Chem. Commun. (2002) 2058-2059.
[9] P. Miedziak, M. Sankar, N. Dimitratos, J.A. Lopez-Sanchez, A.F. Carley, D.W. Knight, S.H. Taylor, C.J. Kiely, G.J. Hutchings, Catal. Today 164 (2011) 315-319.
[10] D.I. Enache, J.K. Edwards, P. Landon, B. Solsona-Espriu, A.F. Carley, A.A. Herzing, M. Watanabe, C.J. Kiely, D.W. Knight, G.J. Hutchings, Science 311 (2006) 362-365.
[11] Q. He, P.J. Miedziak, L. Kesavan, N. Dimitratos, M. Sankar, J.A. Lopez-Sanchez, M.M. Forde, J.K. Edwards, D.W. Knight, S.H. Taylor, C.J. Kiely, G.J. Hutchings, Faraday Discussions (2013).
[12] J.K. Edwards, B.E. Solsona, P. Landon, A.F. Carley, A. Herzing, C.J. Kiely, G.J. Hutchings, J. Catal. 236 (2005) 69-79.
[13] J.K. Edwards, J. Pritchard, L. Lu, M. Piccinini, G. Shaw, A.F. Carley, D.J. Morgan, C.J. Kiely, G.J. Hutchings, Angew. Chem., Int. Ed. 53 (2014) 2381-2384.
[14] J.K. Edwards, J. Pritchard, P.J. Miedziak, M. Piccinini, A.F. Carley, Q. He, C.J. Kiely, G.J. Hutchings, Catal. Sci. Technol. 4 (2014) 3244-3250.
[15] S.-J. Lee, A. Gavriilidis, J. Catal. 206 (2002) 305-313.
[16] M. Sankar, Q. He, M. Morad, J. Pritchard, S.J. Freakley, J.K. Edwards, S.H. Taylor, D.J. Morgan, A.F. Carley, D.W. Knight, C.J. Kiely, G.J. Hutchings, ACS Nano 6 (2012) 6600-6613.
[17] L. Delannoy, N. El Hassan, A. Musi, N.N.L. To, J.-M. Krafft, C. Louis, J. Phys. Chem. B 110 (2006) 22471-22478.
[18] F.o. Moreau, G.C. Bond, A.O. Taylor, J. Catal. 231 (2005) 105-114.
[19] F. Porta, L. Prati, M. Rossi, S. Coluccia, G. Martra, Catal. Today 61 (2000) 165-172.
[20] M.M. Forde, R.D. Armstrong, R. McVicker, P.P. Wells, N. Dimitratos, Q. He, L. Lu, R.L. Jenkins, C. Hammond, J.A. Lopez-Sanchez, C.J. Kiely, G.J. Hutchings, Chem. Sci. 5 (2014) 3603-3616.
[21] S.A. Kondrat, G. Shaw, S.J. Freakley, Q. He, J. Hampton, J.K. Edwards, P.J. Miedziak, T.E. Davies, A.F. Carley, S.H. Taylor, C.J. Kiely, G.J. Hutchings, Chem. Sci. 3 (2012) 2965-2971.
[22] A.A. Herzing, M. Watanabe, J.K. Edwards, M. Conte, Z.-R. Tang, G.J. Hutchings, C.J. Kiely, Faraday Discuss. 138 (2008) 337-351.
[23] M.M. Schubert, S. Hackenberg, A.C. van Veen, M. Muhler, V. Plzak, R.J. Behm, J. Catal. 197 (2001) 113-122.
[24] M. Sankar, E. Nowicka, R. Tiruvalam, Q. He, S.H. Taylor, C.J. Kiely, D. Bethell, D.W. Knight, G.J. Hutchings, Chem. - Eur. J. 17 (2011) 6524-6532.
[25] G. Ertl, H. Knözinger, F. Schüth, J. Weitkamp, Handbook of Hetergenous Catalysis, 2nd addition, Wiley-VCH, 2008
[26] J. Guzman, A. Corma, Chem. Commun. (2005) 743-745.
[27] S. Carrettin, P. Concepcion, A. Corma, J.M. Lopez Nieto, V.F. Puntes, Angew. Chem., Int. Ed. 43 (2004) 2538-2540.
[28] Z.-R. Tang, J.K. Edwards, J.K. Bartley, S.H. Taylor, A.F. Carley, A.A. Herzing, C.J. Kiely, G.J. Hutchings, J. Catal. 249 (2007) 208-219.
[29] P.J. Miedziak, Z. Tang, T.E. Davies, D.I. Enache, J.K. Bartley, A.F. Carley, A.A. Herzing, C.J. Kiely, S.H. Taylor, G.J. Hutchings, J. Mater. Chem. 19 (2009) 8619-8627.

[30] G.J. Hutchings, J.K. Bartley, J.M. Webster, J.A. Lopez-Sanchez, D.J. Gilbert, C.J. Kiely, A.F. Carley, S.M. Howdle, S. Sajip, S. Caldarelli, C. Rhodes, J.C. Volta, M. Poliakoff, J. Catal. 197 (2001) 232-235.
[31] R.P. Marin, S.A. Kondrat, R.K. Pinnell, T.E. Davies, S. Golunski, J.K. Bartley, G.J. Hutchings, S.H. Taylor, Appl. Catal., B 140-141 (2013) 671-679.
[32] Z.R. Tang, S.A. Kondrat, C. Dickinson, J.K. Bartley, A.F. Carley, S.H. Taylor, T.E. Davies, M. Allix, M.J. Rosseinsky, J.B. Claridge, Z. Xu, S. Romani, M.J. Crudace, G.J. Hutchings, Catal. Sci. Technol. 1 (2011) 64-70.
[33] M.E. Tadros, C.L.J. Adkins, E.M. Russick, M.P. Youngman, J. Supercrit. Fluids 9 (1996) 172-176.
[34] T. Lu, S. Blackburn, C. Dickinson, M.J. Rosseinsky, G. Hutchings, S. Axon, G.A. Leeke, Powder Technol. 188 (2009) 264-271.
[35] E. Reverchon, G. Caputo, S. Correra, P. Cesti, J. Supercrit. Fluids 26 (2003) 253-261.
[36] R. Sui, A.S. Rizkalla, P.A. Charpentier, Langmuir 21 (2005) 6150-6153.
[37] Z.-R. Tang, J.K. Bartley, S.H. Taylor, G.J. Hutchings, Stud. Surf. Sci. Catal. 162 (2006) 219-226.
[38] R.P. Marin, S.A. Kondrat, T.E. Davies, D.J. Morgan, D.I. Enache, G.B. Combes, S.H. Taylor, J.K. Bartley, G.J. Hutchings, Catal. Sci. Technol. 4 (2014) 1970-1978.
[39] S.A. Kondrat, S.H. Taylor, Catalysis 26 (2014) 218-248.
[40] R. Sui, A.S. Rizkalla, P.A. Charpentier, J. Phys. Chem. B 110 (2006) 16212-16218.
[41] D.A.H. Hanaor, C.C. Sorrell, J. Mater. Sci. 46 (2011) 855-874.
[42] R.I. Bickley, T. Gonzalez-Carreno, J.S. Lees, L. Palmisano, R.J.D. Tilley, Journal of Solid State Chemistry 92 (1991) 178-190.
[43] J.T. Carneiro, T.J. Savenije, J.A. Moulijn, G. Mul, The Journal of Physical Chemistry C 115 (2011) 2211-2217.
[44] G. Munuera, V. Rives-Arnau, A. Saucedo, Journal of the Chemical Society, Faraday Transactions 1: Physical Chemistry in Condensed Phases 75 (1979) 736-747.
[45] A.A. Gribb, J.F. Banfield, Am. Mineral. 82 (1997) 717-728.
[46] H. Zhang, J.F. Banfield, J. Mater. Chem. 8 (1998) 2073-2076.
[47] J.K. Edwards, J. Pritchard, M. Piccinini, G. Shaw, Q. He, A.F. Carley, C.J. Kiely, G.J. Hutchings, J. Catal. 292 (2012) 227-238
[48] J.K. Edwards, B. Solsona, E.N. N, A.F. Carley, A.A. Herzing, C.J. Kiely, G.J. Hutchings, Science (2009) 1037-1041.

Table 1: Properties of SAS precipitated titanium precursor salts before and after calcination at 450°C

Ti precursor	Surface area (m^2g^{-1})		Phase[b]	Crystalite size[c] (nm)
	Precipitated	Calcined[a]		
Ti-ethoxide	304	76 (30%)	anatase	16
Ti-isopropoxide	254	91 (35%)	anatase (2% rutile)	13
Ti-butoxide	180	54 (25%)	anatase	21
TiO-acetylacetonate	87	33 (38%)	anatase (2% rutile)	14
Anatase	-	20	anatase	61

[a] Values in brackets show percentage retention of surface area on calcination. [b] Determined by XRD analysis. [c] Calculated from XRD using the Scherrer equation.

Table 2: XPS determined atomic concentrations, Pd/Au and Ti/O ratios.

	Element	%At Conc	Pd/Au	Ti/0
$AuPd/TiO_2$(P-25)	Pd 3d	3.11	17.79	0.45
	O 1s	64.57		
	Ti 2p	29.08		
	Cl 2p	3.04		
	Au 4f	0.17		
$AuPd/TiO_2$ (isopropoxide-450 °C)	Pd 3d	2.56	11.69	0.42
	O 1s	66.74		
	Ti 2p	28.36		
	Cl 2p	2.14		
	Au 4f	0.21		
$AuPd/TiO_2$ (isopropoxide-750 °C)	Pd 3d	4.26	32.27	0.41
	O 1s	65.24		
	Ti 2p	26.93		
	Cl 2p	3.43		
	Au 4f	0.13		

Table 3: The results of the synthesis and hydrogenation of hydrogen peroxide by gold-palladium supported on various titania

Catalyst	Calcination temperature (°C)	Calcination time (h)	H_2O_2 Productivity ($molkg^{-1}h^{-1}$)	H_2O_2 hydrogenation (%)
$AuPd/TiO_2$ (P-25)	As received	As received	64	12
$AuPd/TiO_2$ (isopropoxide-450 °C)	450	2	135	7
$AuPd/TiO_2$ (isopropoxide-750 °C)	750	1.5	108	14

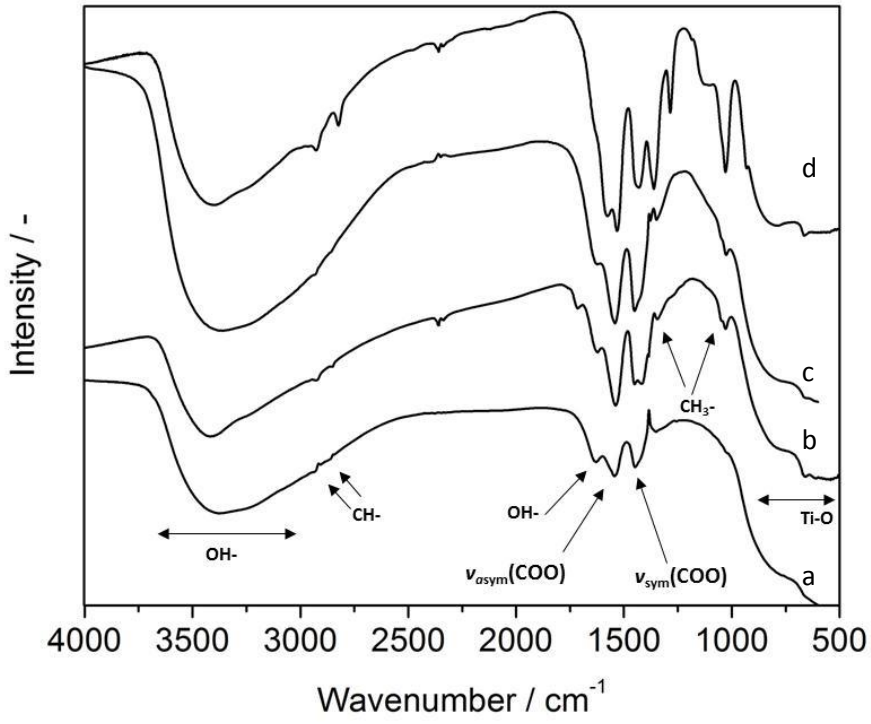

Figure 1. Diffuse reflectance infrared Fourier transform spectroscopy of SAS precipitates. Precursors used: (a) Ti-ethoxide, (b) Ti-isopropoxide, (c) Ti-butoxide and (d) TiO-acetylacetonate

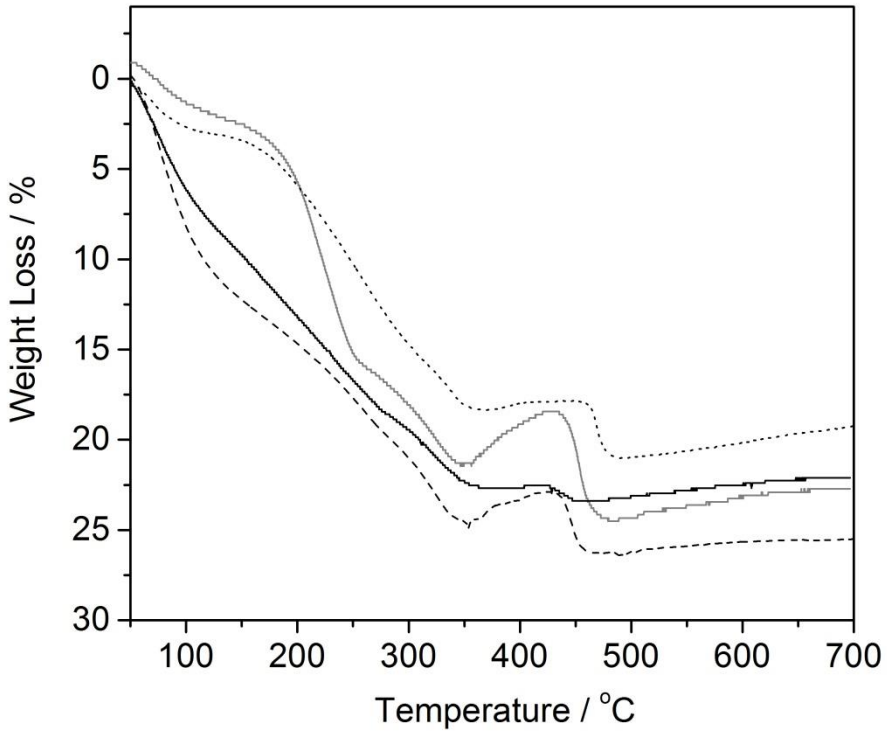

Figure 2. Thermogravimetric analysis of SAS precipitates. Precursors used: (solid black line) Ti-ethoxide, (dotted line) Ti-isopropoxide, (dashed line) Ti-butoxide and (grey line) TiO-acetylacetonate

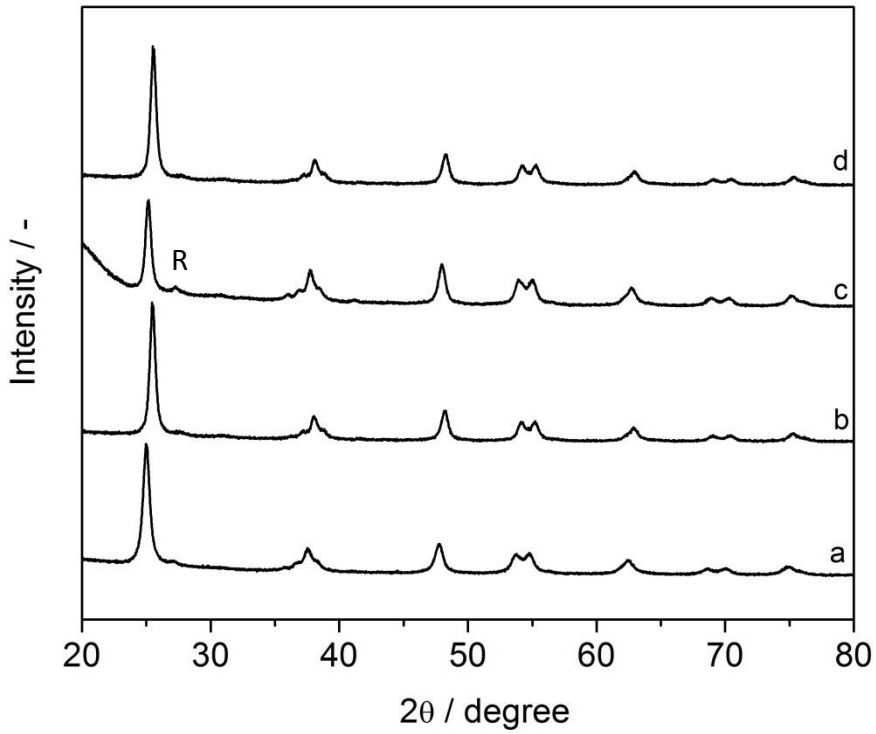

Figure 3. XRD of SAS precipitates calcined at 450 °C for 2h. Derived from precursors: (a) TiO-acetylacetonate (b) Ti-ethoxide, (c) Ti-isopropoxide, and (d) Ti-butoxide . R indicates (110) rutile reflection.

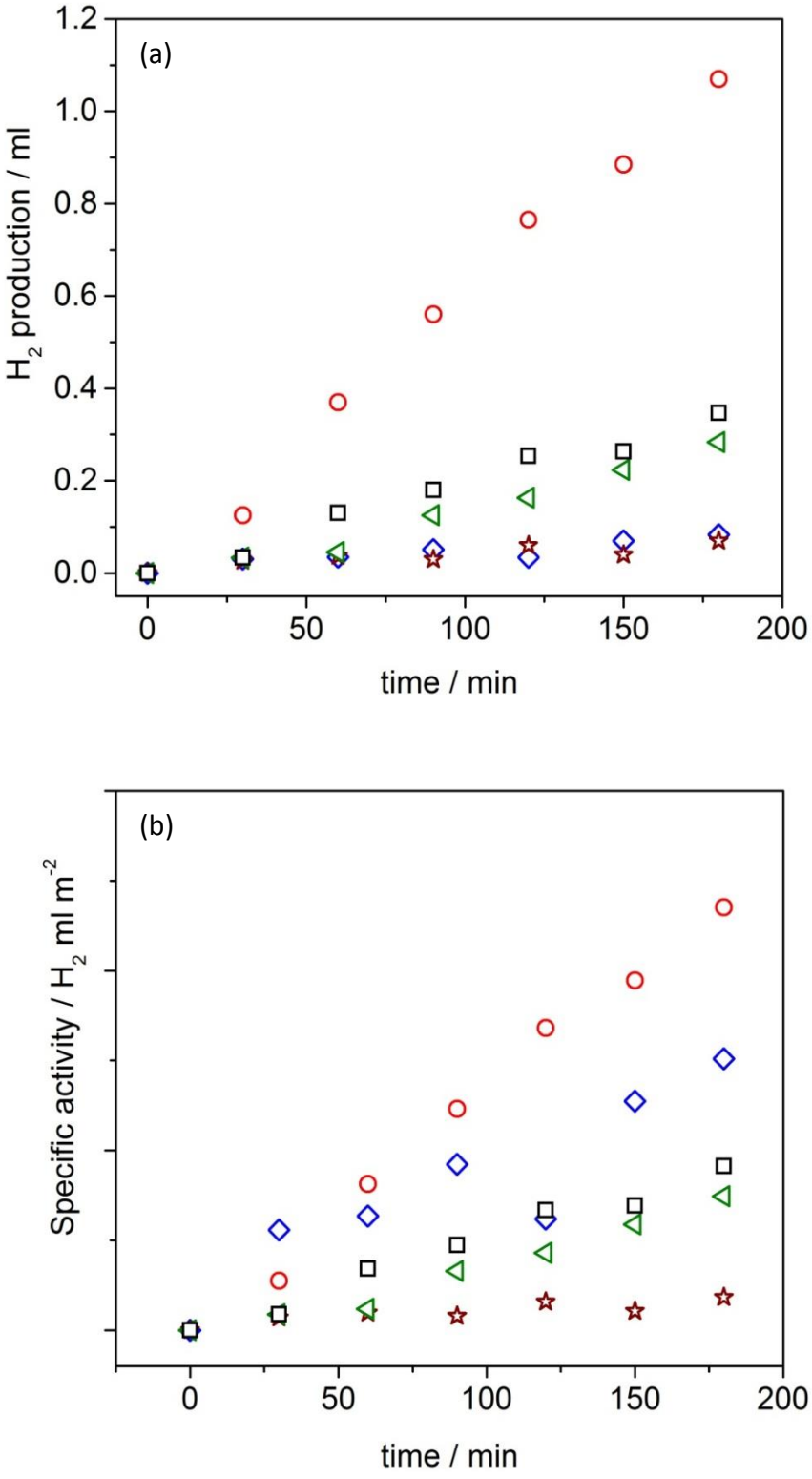

Figure 4. Photocatalytic reactivity of Pt/TiO_2 of SAS derived TiO_2 in the water splitting reaction. TiO_2 prepared from SAS precursors with 450 °C calcination △ Ti-ethoxide, ○Ti-isopropoxide, ☆Ti-butoxide, ◊ TiO-acetylacetonate and □ Anatase standard.

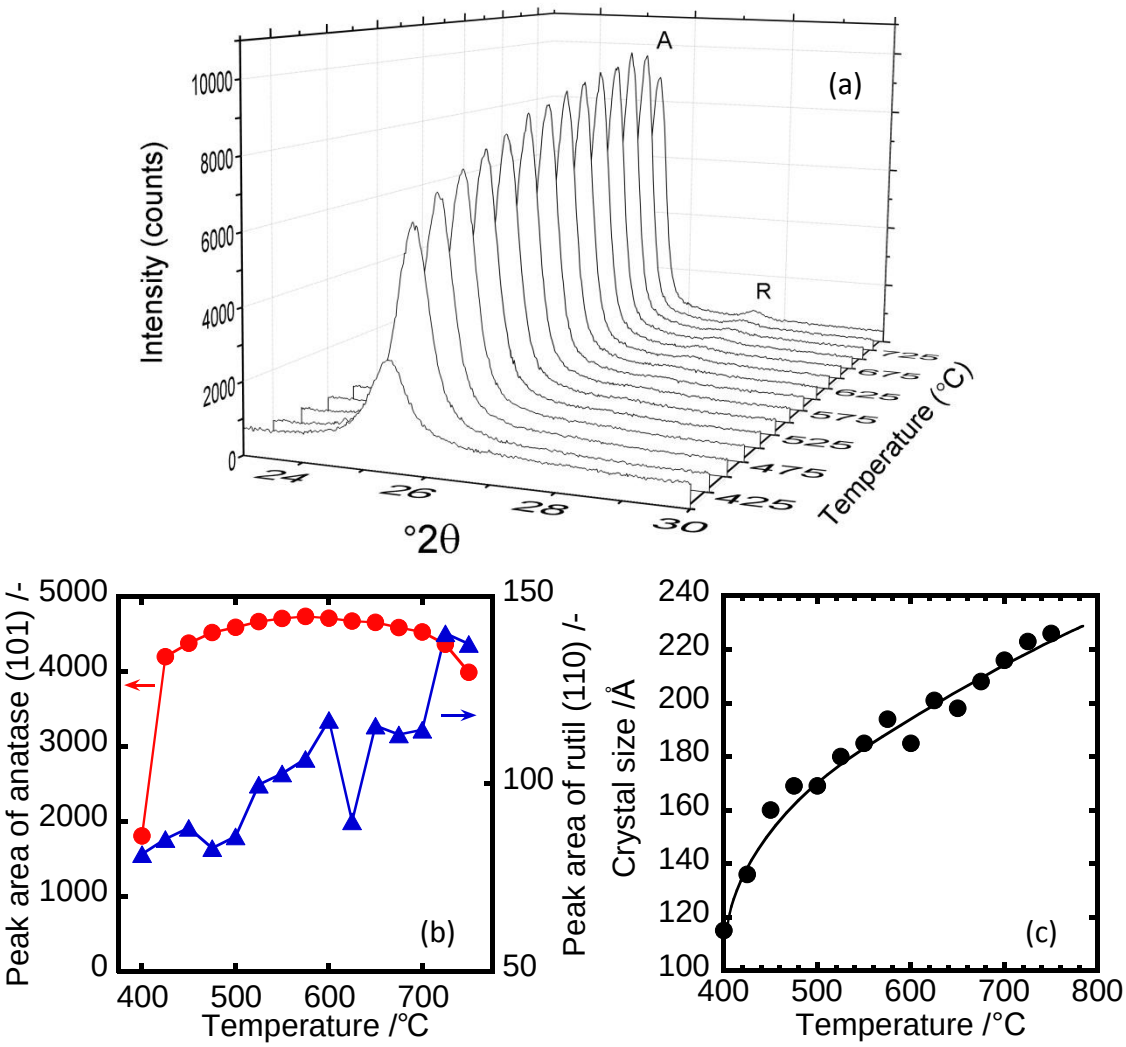

Figure 5. *In* situ XRD analysis of SAS precipitated Ti-isopropoxide calcined from 400 to 750 °C. Ramp rate of 10 °C min^{-1} with scans every 25 °C. The sample was held at each desired temperature for 15 min prior to the scan over the range 2θ = 23-30°. (a) Diffraction patterns with A denoting anatase (101) and R rutile (110). (b) Peak area analysis of (101) anatase and (110) rutile. (c) Evolution of anatase crystallite size with temperature.

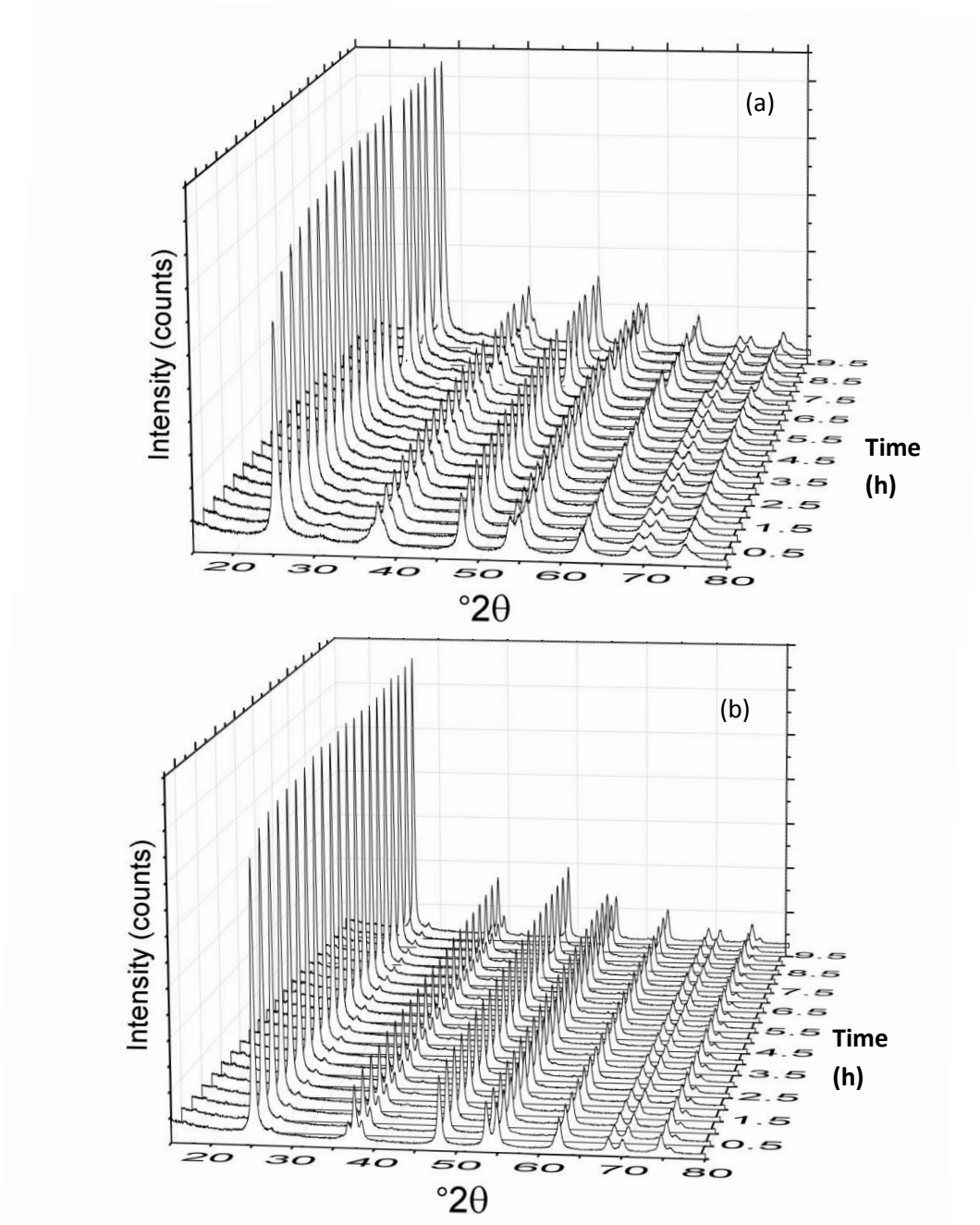

Figure 6. *In* situ XRD analysis of SAS precipitated Ti-isopropoxide isothermal heat treatment experiments at (a) 450 °C and (b) 650 °C . Scans between 10-80° 2θ were taken every 30min.

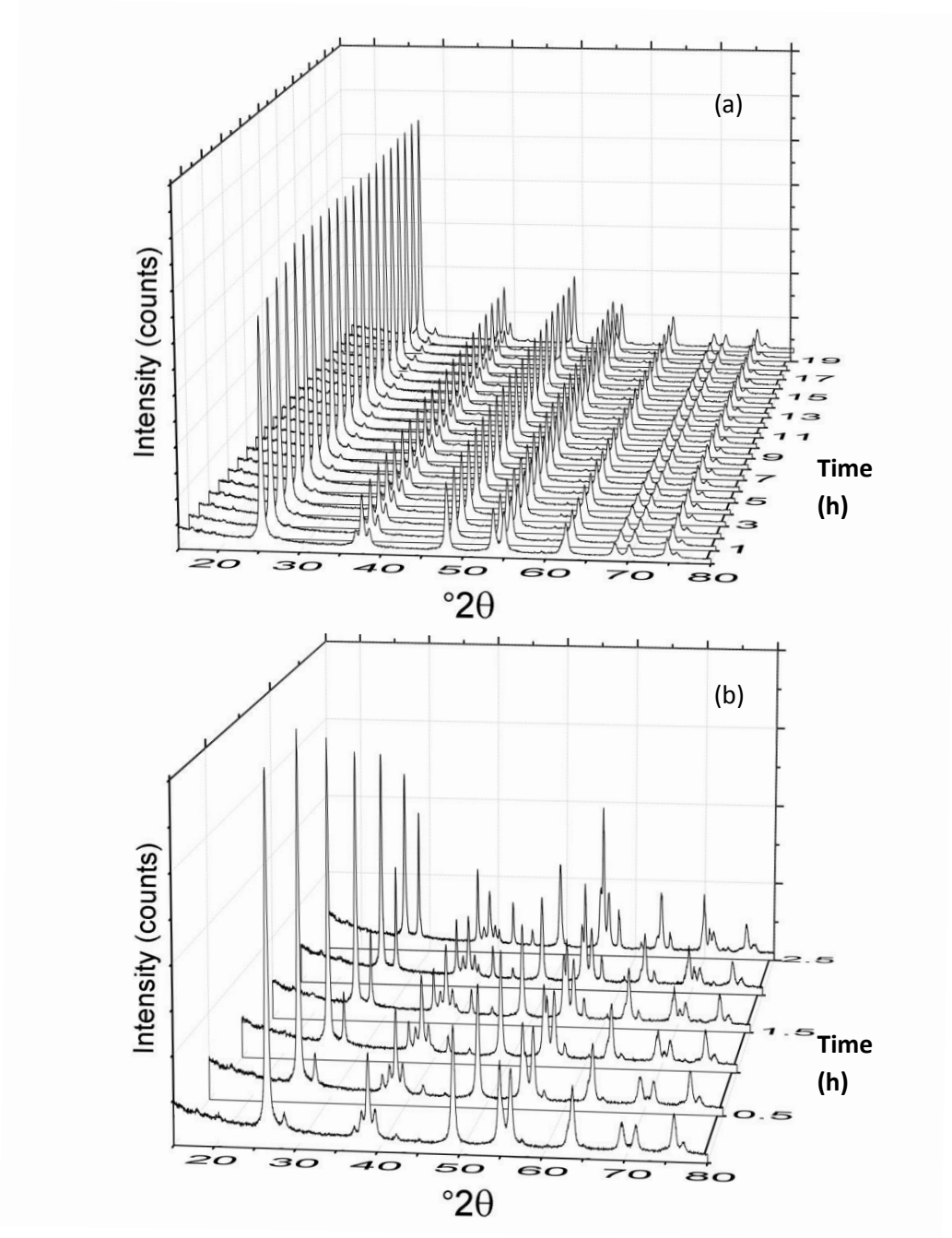

Figure 6. *I In* situ XRD analysis of SAS precipitated Ti-isopropoxide isothermal heat treatment experiments at (a) 700 °C and (b) 750 °C. Scans between 10-80° 2θ were taken every 30 min.

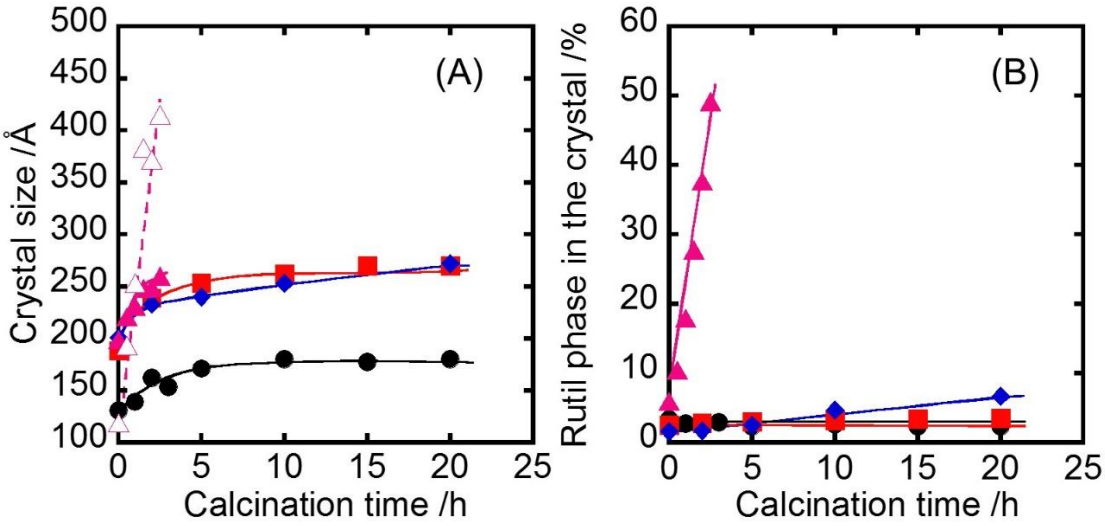

Figure 7 . (A) Crystal size of SAS precipitated Ti-isopropoxide derived TiO_2 obtained by *in situ* XRD and estimated by Sherrer method. Closed circle, 450 °C; closed square, 650 °C; closed lozenge, 700 °C; closed triangle, 750 °C; open triangle, crystal size of rutile phase at 750 °C. (B) rutile phase content. Closed circle, 450 °C; closed square, 650 °C; closed lozenge, 700 °C; closed triangle, 750 °C.

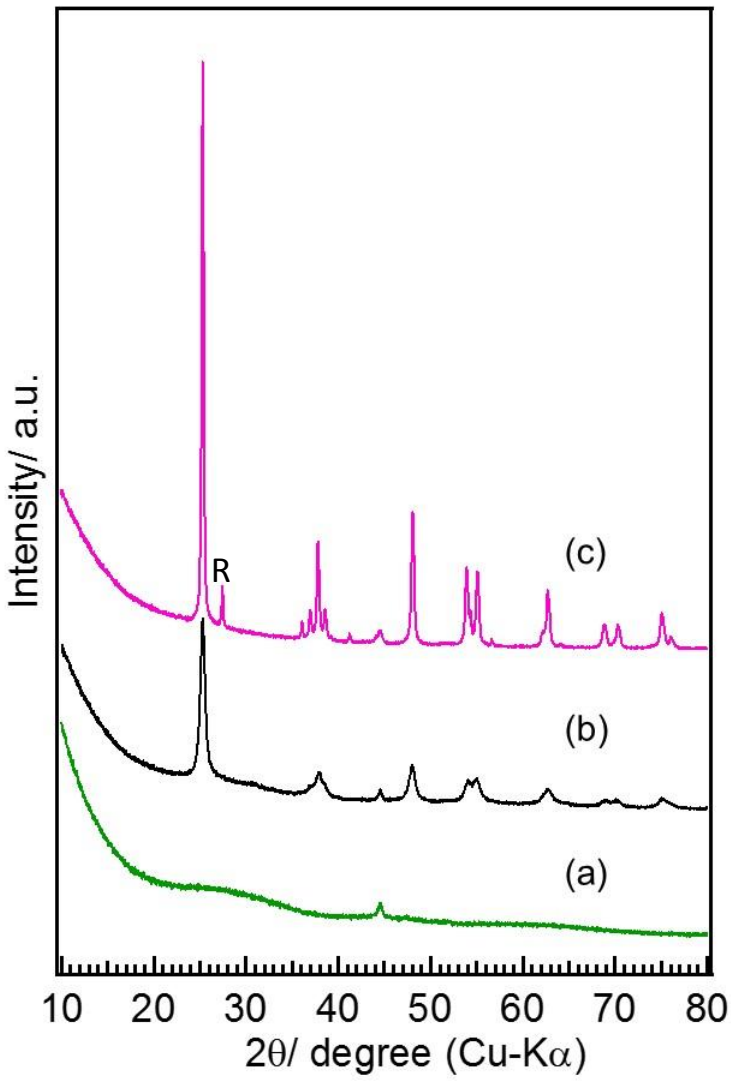

Figure 8 . XRD pattern of (a) Ti-isopropoxide , (b) Ti-isopropoxide ex-situ calcined 450 °C, and (c) Ti-isopropoxide ex-situ calcined 750 °C. R denoting rutile (110).

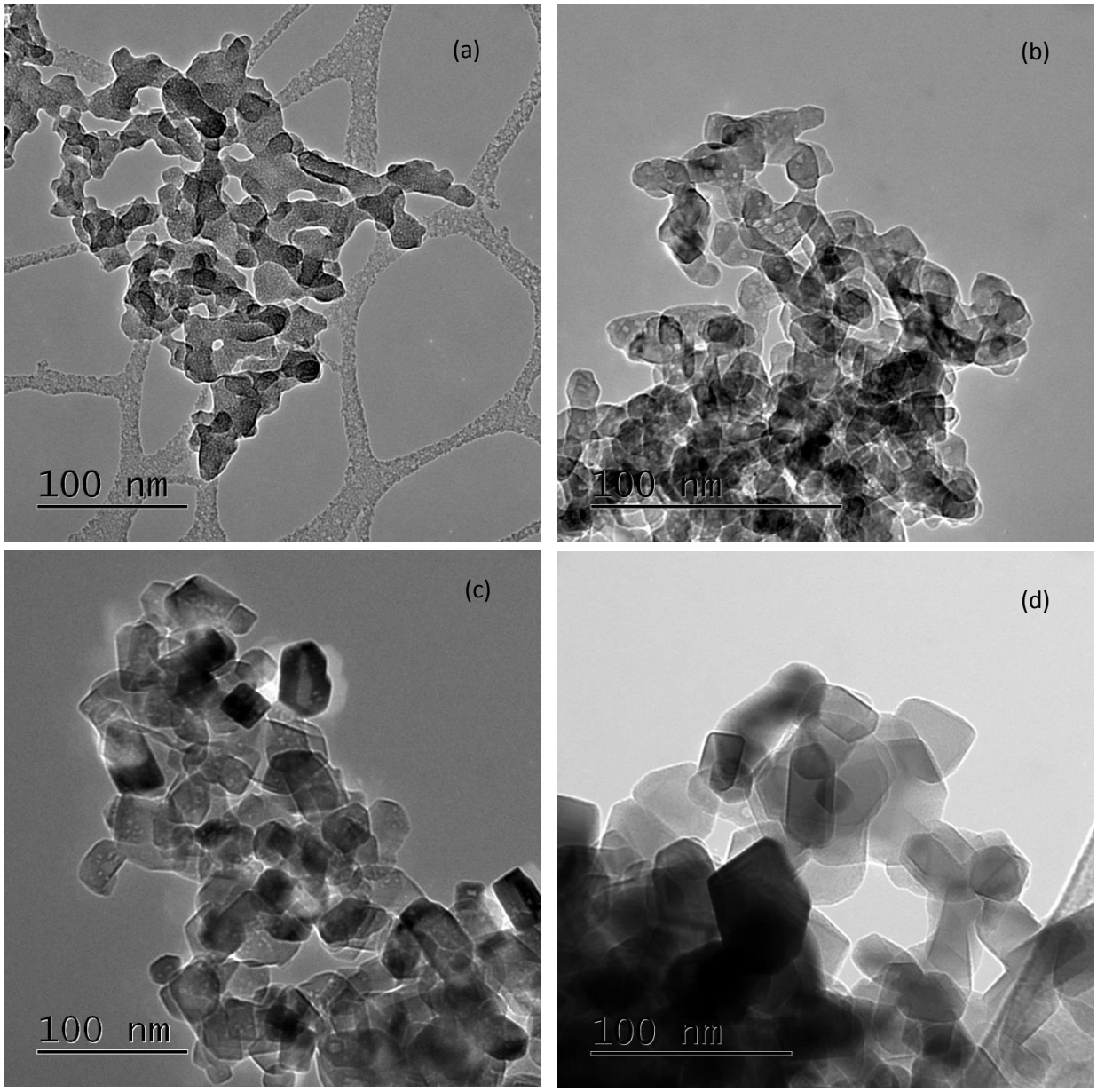

Figure 9. Representative TEM images of (a) Ti-isopropoxide SAS precipitate and after (b) 450 °C calcination, (c) 650 °C calcination, (d) 750 °C calcination.

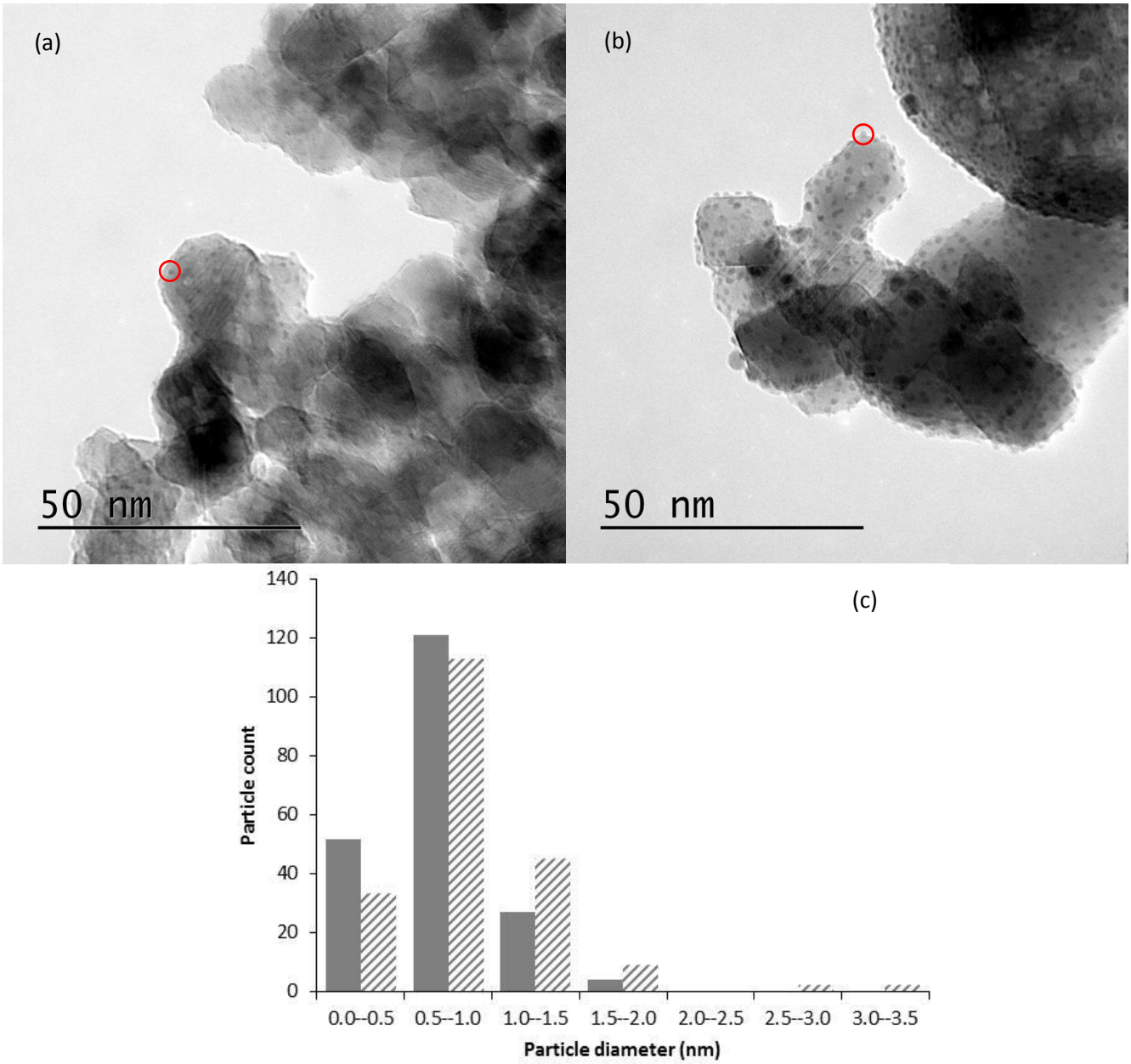

Figure 10. Representative TEM images of 5wt% AuPd/TiO_2 prepared from Ti-isopropoxide SAS precipitate calcined at (b) 450 °C, (b) 750 °C calcination. The highlighted areas in red highlight a metal nanoparticle. (c) Particle size distribution of 5wt% AuPd/TiO_2 450 °C calcination (grey bar) and 5wt% AuPd/TiO_2 750 °C calcination (dashed bar).

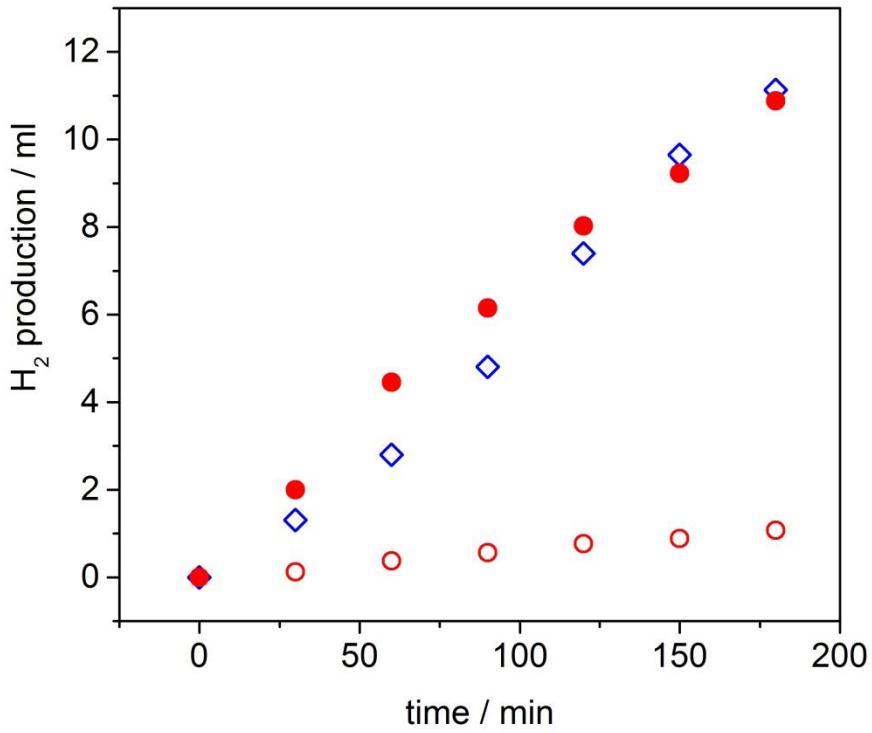

Figure 11. Photocatalytic reactivity for water splitting with Pt/TiO_2 of Ti-isopropoxide SAS derived TiO_2 calcined at different temperatures and comparable data for a standard $Pt/P\text{-}25$ TiO_2 catalyst. SAS Ti-isopropoxide calcined at 450 °C (○) containing 2 wt% rutile and 750 °C (●) containing 10 wt% rutile. (◇) Catalyst prepared with commercial P-25 containing 20 wt% rutile.

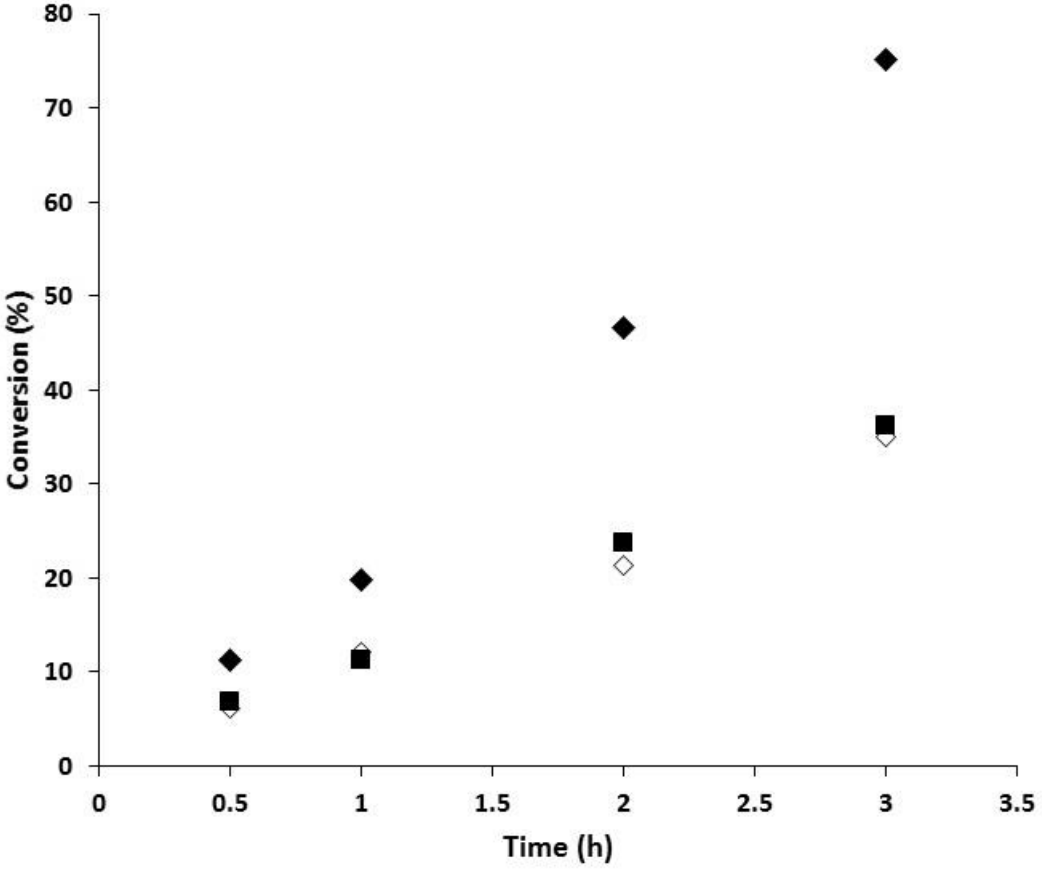

Figure 12: The conversion of benzyl alcohol AuPd/TiO_2(P-25), squares; AuPd/TiO_2(isopropoxide450°C), open diamonds; AuPd/TiO_2(isopropoxide450°C)closed diamonds.

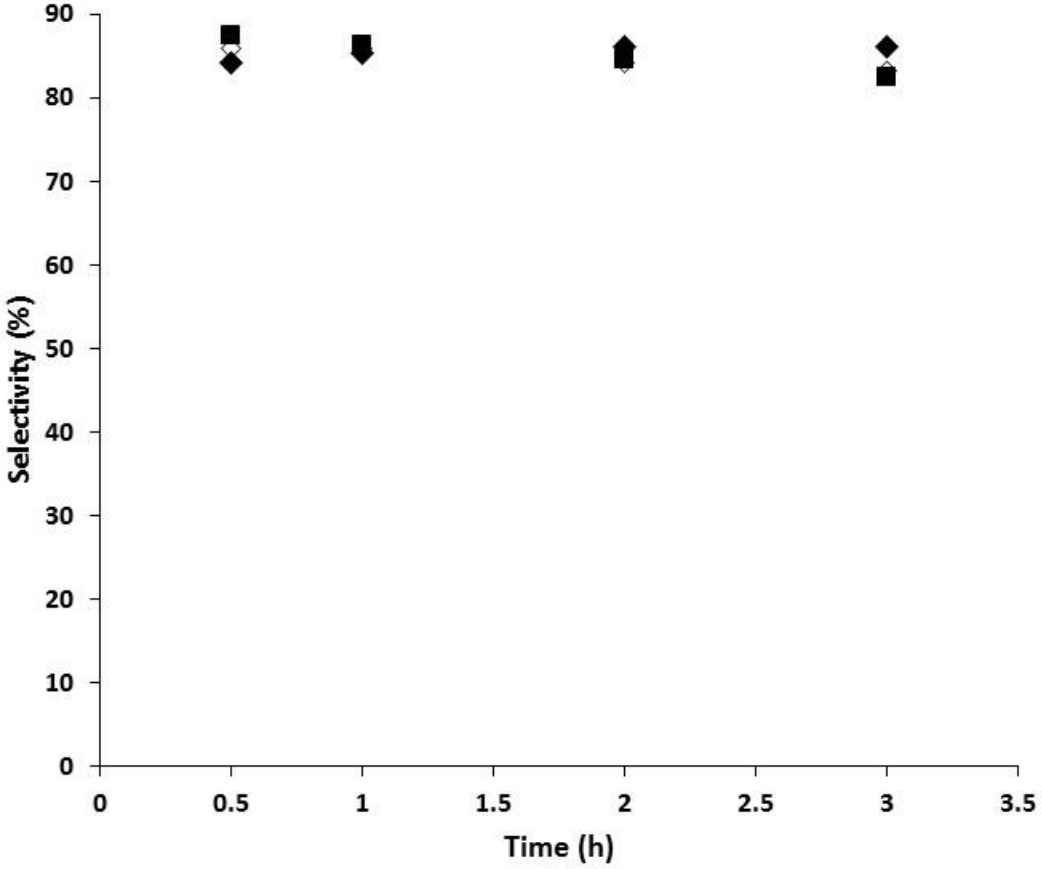

.

Figure 13: The selectivity towards benzaldehde during the oxidation of benzyl alcohol, AuPd/TiO_2(P-25), squares; AuPd/TiO_2(isopropoxide450°C), open diamonds; AuPd/TiO_2(isopropoxide450°C) closed diamonds.